Differential imaging in coherent anti-Stokes Raman scattering microscopy II: a filter-assisted Laguerre-Gaussian beam detection scheme

Liu Cheng, Suhas P. Veetil, Dug Young Kim

Department of Information and Communications, Gwangju Institute of Science and Technology
Buk-gu, Gwangju, Republic of Korea 500-712
liucheng@gist.ac.kr

Abstract: A new differential imaging technique to obtain contrast improvement in coherent anti-Stokes Raman scattering (CARS) microscopy is proposed through a spatial spiral phase modulation in the collected signal of CARS microscopy. A spiral phase mask makes the CARS signal from the bulk material to be distributed in a ring centered at the detecting pinhole of a confocal microscope resulting in a weak detected CARS signal from a bulk material. When tiny scatters are included in the focal volume of a CARS setup, the ring-shaped distribution of CARS field is distorted, leading to an increase in the detected signal through the pinhole. The sensitivity and the size selectivity of this proposed technique is studied with varying the particle size, and it is found that this method is to be efficient in edge detection. Simulation results obtained by finite difference time domain (FDTD) methods show that the image contrast is enhanced by many times as it is able to highlight the details of the specimen by suppressing the CARS signal from a bulk or a uniform material.

OCIS codes: (290.5860) Scattering Raman; (300.6230) Spectroscopy, Coherent anti-Stokes Raman scattering; (180.1790) Confocal microscopy; (330.6130) Spatial resolution

References:

1. J. X. Cheng and X. S. Xie, "Coherent anti-Stokes scattering microscopy: instrumentation, theory, and application," J. Phys. Chem. B. **108**, 827-840 (2004).
2. J. X. Cheng, A. Volkmer, and X. S. Xie, "Theoretical and experimental characterization of coherent anti-Stokes Raman scattering microscopy," J. Opt. Soc. Am. B. **19**, 1363-1375 (2002).
3. H. Wang, Y. Fu, P. Zickmund, R. Shi, and J. X. Cheng, "Coherent anti-Stokes Raman scattering imaging of axonal myelin in live spinal tissues," Biophysical Journa **l 89**, 581-591 (2005).
4. R. J.H. Clark and R. E. Hester, *Advances in Nonlinear Spectroscopy* (Wiley New York, 1988).
5. P. D. Maker and R. W. Terhune, "Study of optical effects due to an induced polarization third order in the electric field strength," Phys, Rev., A **137** 801-818 (1965).
6. Y. R. Shen, *The principles of nonlinear optics* (Wiley New York, 1984).
7. E. O. Potma, C. L. Evans, and X. S. Xie, "Heterodyne coherent anti-Stokes Raman scattering (CARS) imaging," Opt. Lett. **31**, 241-243 (2006).
8. A. Volkmer, J. X. Cheng, and X. S. Xie, "Vibrational imaging with high sensitivity via epidetected coherent anti-Stokes Raman scattering microscopy," Phys. Rev. Lett. 87, 023901-1-023901-4 (2001).
9. J. X. Cheng, L. D. Book, and X. S. Xie, "Polarization coherent anti-Stokes Raman scattering microscopy," Opt. Lett. **26**, 1341-1343 (2001)
10. J. X. Cheng, Andreas Volkmer, Lewis D. Book, and X. Sunney Xie, "An epi-detected coherent anti-Stokes Raman scattering (E-CARS) microscope with high spectral resolution and high sensitivity," J. Phys. Chem. B, **105**, 1277 -1280 (2001).
11. V. V. Krishnamachari, E. O. Potma, "Focus-engineered coherent anti-Stokes Raman scattering microscopy: a numerical investigation," J. Opt. Soc. Am. A **24**, 1138-1147 (2007).
12. C. Liu, D. Y. Kim, "Differential imaging in coherent anti-Stokes Raman scattering microscopy with Laguerre- Gaussian excitation beams," Opt. Express **15**, 10123-10135 (2007)
13. S. Mukamel, *Principles of Nonlinear Optical Spectroscopy* (Oxford U. Press New York, 1995).

#86014 - $15.00 USD Received 1 Aug 2007; revised 30 Aug 2007; accepted 2 Sep 2007; published 6 Sep 2007

14. R. W. Boyd, *Nonlinear Optics* (Academic Boston, 1992).
15. K. S. Yee, "Numerical solution of initial boundary value problem involving Maxwell equations in isotropic media," IEEE Trans. Antennas Propagat. **14**, 302-307 (1966).
16. A. Taflove, Computational Electrodynamics: *The Finite-Difference Time-Domain Method* (Artech House Boston, 1995).
17. M. Hashimoto, T. Araki, "Three-dimensional transfer functions of coherent anti-Stokes Raman scattering microscopy," J. Opt. Soc. Am. A **18**,771-776 (2001)
18. S. Fürhapter, A. Jesacher, S. Bernet, and M. Ritsch-Marte, "Spiral phase contrast imaging in microscopy," Opt. Express **13**, 689-694 (2005)
19. J. A. Davis, D. E. McNamara, D. M. Cottrell, and J. Campos, "Image processing with the radial Hilbert transform: theory and experiments," Opt. Lett. 25, 99–101 (2000).

1. Introduction

Coherent anti-Stokes Raman Scattering (CARS) microscopy is increasingly being utilized in biological imaging due to its strong optical sectioning capability and excellent chemical selectivity [1-3]. On excitation with a pumping light of frequency ω_p and Stokes light of frequency ω_s , the molecules with vibration energy level equal to $\omega_p - \omega_s$ are resonantly excited and radiate CARS signal of frequency $\omega_{as} = 2\omega_p - \omega_s$. This signal is used for chemical mapping of the biological sample in CARS microscopy. Due to the coherence properties of the CARS, the microscopic image detected in the forward direction always suffers from strong non-resonant background from the solvent water of the bio-samples, which carries no chemical information of the sample and always overwhelms the signal from small scatters [4-6]. In an epi-detection mode, the CARS waves emitted from different points in the focal volume always destructively interfere unless interface or sub-wavelength structures are present, leading to the CARS image which is free from non-resonant background and shows strong size selectivity [7-10]. Epi-CARS microscope has proven powerful for high contrast imaging of cellular membrane and other small organelles. However, the interference effect in the epi-CARS is prominent only along the direction of the optical axis rather than in the lateral direction; hence it is not sensitive to the nonlinear coefficient variations in the lateral dimensions.

Since differentiating different cellular features in the focal plane is always attractive for bio-imaging, a spiral phase excitation method was proposed to realize differential imaging for interface highlighting and contrast improvement in CARS microscopy [11, 12]. This method used higher order Gaussian or Laguerre-Gaussian input modes which are assumed to be generated from propagating Gaussian beams by using spiral phase modulator. The principle behind the method is to create a π- phase jump in the exciting lights and there by a π- phase discontinuity in the CARS field such that the CARS signals from different points in the focal volume can destructively interference with each other and can result in a very weak intensity. When materials with different third-order nonlinearities are present, the phase distribution is distorted and the detected intensity becomes strong. Theoretically, these methods have a strong ability in highlighting the details of the sample. However, it is not easy to realize for practical applications. First of all, to obtain higher order Gaussian beams, a spatial phase modulator is to be used to imprint a spiral shaped phase profile on the exciting beams. However the spectral distance between the pumping and the Stokes lights, which is determined by the Raman shift of the target molecule, is always larger than 100nm for imaging bio-samples, and it is not easy to modulate both the pumping and the Stokes beams simultaneously with one spatial phase modulator due to its limited spectral response range and related color dispersion. On the other hand, when a beam such as an LG01 mode is used as an excitation beam, the intensity at the center is zero and most of the energy is distributed in a ring in the focal volume. Since the peak intensity of such focal spot is ten times lower than that of a tight focus, the efficiency of the CARS generation would be seriously reduced. Further more, when Laguerre-Gaussian beam is used for excitation, the size of the focal spot

#86014 - $15.00 USD Received 1 Aug 2007; revised 30 Aug 2007; accepted 2 Sep 2007; published 6 Sep 2007

is always two times larger than that of a Gaussian beam. This means that the high image contrast of Laguerre-Gaussian excitation is obtained at the expense of a decrease in spatial resolution and CARS generation. Additionally, the high energy of the excitation beam used in CARS microscopy may damage the fragile liquid crystal of the phase modulator.

We have found that a modification to the CARS detection scheme which is presented in our earlier paper [12] can resolve the disadvantages mentioned above. In this second paper, we discuss the background suppression and contrast improvement by modulating the spatial phase distribution of the excited CARS signal just before it is detected, instead of modulating the illuminating signal itself as reported earlier. With this kind of scheme the sample is uniformly illuminated so that it does not lead to a decrease in either the excitation efficiency or the spatial resolution. In addition, since the CARS signal is only a monochromic light in the visible range, most of the commonly used spatial phase modulator can be applied for this scheme. This makes the differential CARS microscopic imaging much more suitable for practical application. Further more, any possible damage to the phase modulator is also prevented since the exciting beams are removed from the signal before it is passed through the phase modulator.

2. Simulation setup

The schematic of the simulation setup is in Fig. 1. The pump beam is assumed to be at a wavelength of 750 nm and the Stokes beam at 852 nm. The beams are combined together with a dichroic mirror and focused by an objective with a numerical aperture (NA) of 0.7 to excite the specimen. The generated CARS signal is collected by a modified confocal system. A spatial phase modulator with a spiral-phase distribution is placed after the band pass filter to modulate the CARS signal. The sample medium is assumed to be polystyrene particles in water and is fixed on a translational stage driven by PZT.

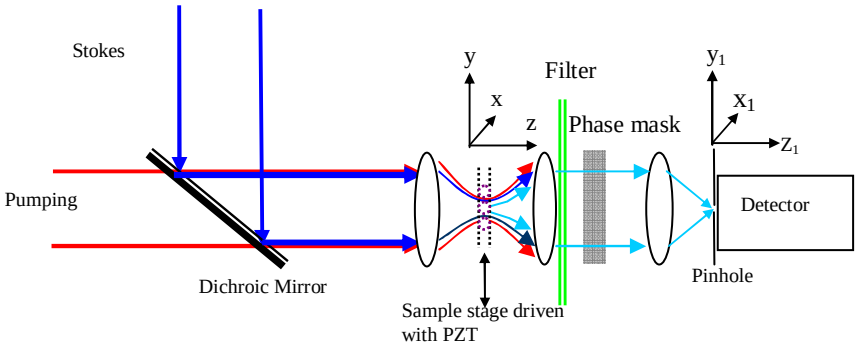

Fig. 1 Simulation setup

3. Finite-Difference Time-Domain (FDTD) method

The generation and propagation of the CARS field in a homogeneous and isotropic medium are governed by the wave equation [13, 14].

$$\nabla\times\nabla\times \mathrm{E}(\mathrm{r},\mathrm{t})+\frac{n^2}{c^2}\frac{\partial E(\mathbf{r},\mathrm{t})}{\partial \mathrm{t}^2}=-\frac{4\pi}{c^2}\frac{\partial^2 \mathrm{P}^{(3)}(\mathrm{r},\mathrm{t})}{\partial^2 \mathrm{t}} \tag{1}$$

where $P^{(3)}(r,t)$ is the third-order nonlinear polarization, n is the refractive index of the medium for the signal field, and c is the velocity of light in vacuum. The third-order polarization at the anti- Stokes frequency ω_{as} can be written as [4]

$$P_i^{(3)}(\mathrm{r},\omega_{as},t)=3\sum_{jkl}\chi_{ijkl}^{(3)}E_j^{P}(\mathrm{r},\omega_p,t)E_k^{P}(r,\omega_p,t)E_l^{S^*}(\mathrm{r},\omega_s,t) \tag{2}$$

#86014 - $15.00 USD Received 1 Aug 2007; revised 30 Aug 2007; accepted 2 Sep 2007; published 6 Sep 2007

where $\chi^{(3)}_{ijkl}$ is the third-order nonlinear coefficient of a medium. The time-dependant amplitude of pump beam and Stokes beam are represented by $E_j^P(\mathrm{r},\omega_p,t)$, $E_k^P(r,\omega_p,t)$ and $E_l^{S^*}(\mathrm{r},\omega_s,t)$. Indices *j*, *k* and *l* show the directions. If the distributions of the excitation light fields (pump and Stokes beams) and the third-order nonlinear coefficient are known, the third-order nonlinear polarization at different directions can be determined using Eq. (2), and then the CARS distribution could be derived by solving Eq. (1).

Theoretically, the generation and propagation of CARS signal of any specimen can be determined by Eq. (1) and Eq. (2); however, due to the complexity involved in determining the boundary conditions, it is impossible to explicitly determine the excitation light fields and the induced nonlinear polarization in most of experimental situations. To resolve this problem, we propose to use the Finite Difference Time Domain (FDTD) method to simulate the induced nonlinear polarization and the CARS scattering [15].

In the absence of free electric charge and current source in a medium of interest, the Maxwell equations can be written as [16].

$$\begin{cases} \nabla \times H = \dfrac{\partial D}{\partial t} \\ \nabla \times E = -\dfrac{\partial B}{\partial t} \end{cases} \tag{3}$$

where H, D, E**,** and B stand for magnetic field, electric displacement, electric field, and magnetic flux density, respectively. In FDTD simulations, Eq. (3) is discretized with standard staggered grids in temporal and spatial domains. The discretized equations for time dependent electric fields in the FDTD simulator for 3-D coordinates are as follows [15, 16]:

$$\begin{cases} E_x^{n+1}(i+0.5,\,j,\,k) = A(m)\cdot E_x^{n}(i+0.5,\,j,\,k) + B(m)[(H_z^{n+0.5}(i+0.5,\,j+0.5,\,k) - H_z^{n+0.5}(i+0.5,\,j-0.5,\,k))/\Delta y \\ \qquad\qquad - (H_y^{n+0.5}(i+0.5,\,j,\,k+0.5) - H_y^{n+0.5}(i+0.5,\,j,\,k-0.5))/\Delta z \\ E_y^{n+1}(i,\,j+0.5,\,k) = A(m)\cdot E_x^{n}(i,\,j+0.5,\,k) + B(m)[(H_x^{n+0.5}(i,\,j+0.5,\,k+0.5) - H_x^{n+0.5}(i,\,j+0.5,\,k-0.5))/\Delta z \\ \qquad\qquad - (H_y^{n+0.5}(i+0.5,\,j+0.5,\,k) - H_z^{n+0.5}(i-0.5,\,j+0.5,\,k))/\Delta x \\ E_z^{n+1}(i,\,j,\,k+0.5) = A(m)\cdot E_x^{n}(i,\,j,\,k+0.5) + B(m)[(H_y^{n+0.5}(i+0.5,\,j,\,k+0.5) - H_y^{n+0.5}(i-0.5,\,j,\,k+0.5))/\Delta x \\ \qquad\qquad - (H_x^{n+0.5}(i,\,j+0.5,\,k+0.5) - H_x^{n+0.5}(i,\,j-0.5,\,k+0.5))/\Delta y \end{cases} \tag{4}$$

where $A(m) = [2\varepsilon(m) - \sigma(m)\Delta t] = [2\varepsilon(m) + \sigma(m)\Delta t]$ and $B(m) = 2\Delta t/[2\varepsilon(m) + \sigma(m)\Delta t]$. ε is the permittivity of the medium, σ is the conductivity, Δx and Δy are the sampling distance in space and $m = (i\Delta x + j\Delta y + k\Delta z)$. The discretized equations for the magnetic fields in the FDTD simulator can be written similarly to the electric fields as above. After a number of leapfrog iterations using Eq. (4), the electromagnetic field will converge to a stable value determined by the related boundary conditions. Based on this leapfrog approach in time-domain, FDTD simulator will determine not only the steady state parameters (e.g., intensity distribution of light fields, phase and polarization of the localized fields), but also the temporal evolution of these parameters. The FDTD method is utilized to determine the local excitation light field surrounding the scatterers. Knowing the value of the non-linear coefficient, the induced nonlinear polarization can be calculated from Eq. (2). Finally, the scattering pattern of the CARS signals is calculated from the FDTD representation of Eq. (1) by considering the induced nonlinear polarization as an additional radiation source for CARS generation.

#86014 - $15.00 USD Received 1 Aug 2007; revised 30 Aug 2007; accepted 2 Sep 2007; published 6 Sep 2007

4. CARS generation and detection

The coherent transfer function or the complex amplitude of CARS signal in the focal plane (x; y; z) at the detector shown in the set up (Fig. 1) is given by [17]

$$u(x_1, y_1) = \iint P^{(3)}(x, y, \omega_{as})\, g(x_1 - x, y_1 - y)\, dxdy \tag{5}$$

The intensity of the signal at the detector is

$$I_{Det} = \int_{-\delta x}^{\delta x} \int_{-\delta y}^{\delta y} \left| \iint P^{(3)}(x, y, \omega_{as})\, g(x_1 - x, y_1 - y) \mathrm{d}x\mathrm{d}y \right|^2 \mathrm{d}x_1 \mathrm{d}y_1 \tag{6}$$

δx and δy are the sizes of the detector pinhole in x and y directions. $P^{(3)}$ (x, y, ω_{as}) is the induced nonlinear CARS polarization in the focal plane at (x; y; z) and g(x_1; y_1) is the amplitude point spread function of the collecting lens. When a collimated light beam is normally incident on the phase modulator with a spiral phase distribution of the form exp [$i\varphi$] and focused on the plane (x_1; y_1; z_1), the distribution of the focal field or g(x_1; y_1) is remarkably different from that produced by a common lens. φ is the polar angle in a plane transverse to the light propagation direction and it imprints a spiral phase modulation on the transmitted light. A detailed study on the point spread function is given in the next subsection.

4.1 Point spread functions of excitation and collection

For a better understanding of the merits of the setup in Fig. 1, we should know the point spread functions of both the illuminating and collecting lens as they basically determine the distribution of the excitation field and the collection efficiency. Fig. 2(a) and Fig. 2(b) show x- and y- components of the focused field and respective phase distribution inside the bulk sample, water. It is assumed that the incident light is polarized in the x-direction. The intensity of the x-component is much higher than the y-component. Thus only the x-component is considered for simplicity. The focal field of the Stokes light also has a similar distribution and is not shown here.

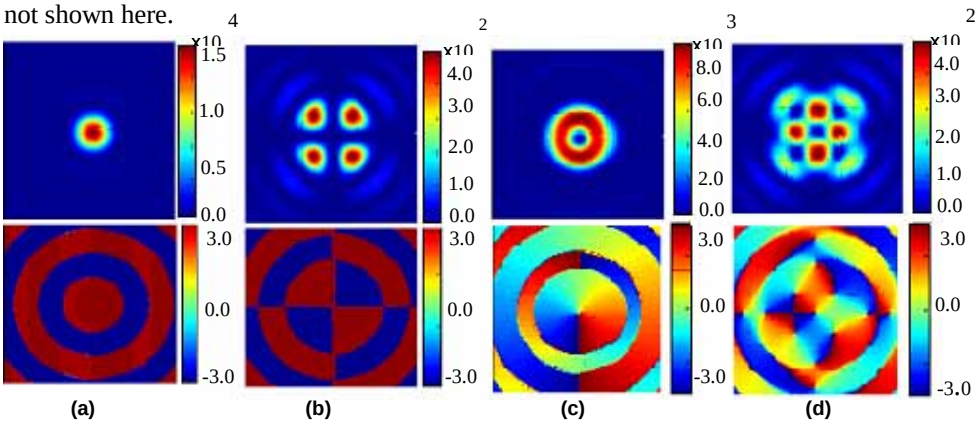

Fig. 2 Point spread functions (PSF) of the illumination and collection lens and the corresponding phase (bottom row). Fig. 2(a) and Fig. 2(b) corresponds to the x and y components of the PSF of the illumination lens and Fig. 2(c) and Fig. 2(d) represents that of collection lens. The size of each figure is 5 μmx5 μm

The point spread function and the phase distribution of the collector lens including the effect of phase mask is shown in Fig. 2(c) and Fig. 2(d). The parameters of the collecting lens are assumed to be the same as that of the illuminating lens. A Gaussian focal field is used for illumination of the sample. It is obvious that the intensity of the x-component is almost zero at the center, and most of its energy is distributed into a ring. The phase distribution is radially antisymmetric with respect to its center. Such a focal spot with zero intensity at the center is used for CARS excitation to suppress the background scattering from uniform (isotropic) bulk

#86014 - $15.00 USD Received 1 Aug 2007; revised 30 Aug 2007; accepted 2 Sep 2007; published 6 Sep 2007

samples [11]. Under such excitation, the CARS signals generated at different points within the focal volume will cancel out in the forward direction. The peak intensity of the collected signal is about three times weaker, and the size of the focal spot is at least two times larger in comparison to the illuminating field. This means that when this kind of focus spot is used for CARS excitation, the efficiency of signal generation will be reduced by a factor of about 27 and the spatial resolution of the microscopy will be decreased by at least a factor of two. This is one of the reasons why the present study suggests using a 'radial staircase' phase modulator for CARS signal collection rather than for CARS excitation.

4.2 Background suppression

When tiny particles are included in the focal volume, the distribution of the excitation fields in Fig. 2(a) would change remarkably by the effects of diffraction, index mismatch, scattering, and the induced nonlinear polarization. In such cases, the amplitude coherent transfer function determined by Eq. (5) would change accordingly. For easy comparison, we first study the generation and detection of CARS signals from a uniform bulk sample, water, with the setup shown in Fig. 1. The water is isotropic with nonlinear coefficient equal to 0.6. The amplitude and the phase distributions of the induced nonlinear polarization at the focal plane (x; y; z) are shown in Fig. 3(a) and Fig. 3(e) respectively, where we can find that both intensity and phase are centro-symmetric with respect to the optic-axis. The amplitude distribution of the CARS signal at the detector plane at (x_1; y_1; z_1) is shown in Fig. 3(i). In the case of an isotropic sample, CARS signal forms a ring at the pinhole of the confocal detection system lying in the optic axis. As most of the light is blocked by the pinhole, the received CARS signal is very weak ie the bulk CARS scattering from the uniform sample can be efficiently suppressed by the proposed technique.

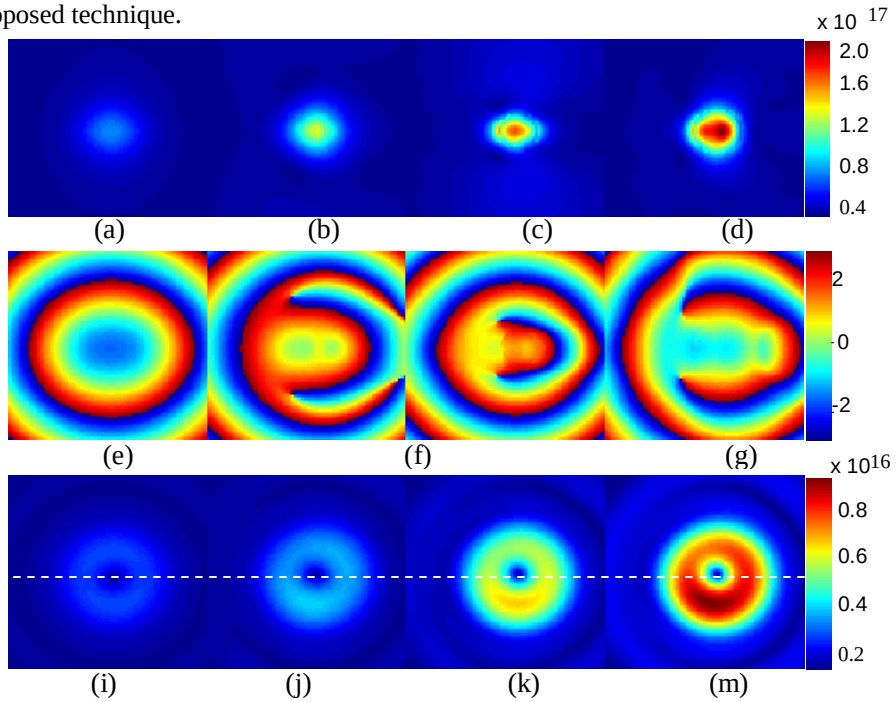

Fig. 3 The variation in nonlinear polarization, coherent transfer function and the corresponding phase modulation for different particle sizes. Fig. 3 (a)-(d) show the nonlinear polarization for water and particles with diameters 200 nm, 320 nm and 400 nm respectively. Fig. 3 (e)-(h) show the corresponding phase modulation and Fig. 3 (i)-(m) show the corresponding coherent transfer function. Phase distribution becomes asymmetric with increase in particle size leading to increased signal detection through the pinhole. The size of each figure is 5 μmx5 μm.

#86014 - $15.00 USD Received 1 Aug 2007; revised 30 Aug 2007; accepted 2 Sep 2007; published 6 Sep 2007

To study the capability of the system in highlighting the details of the specimen, the signal generation and detection are studied by including particles of various sizes in the focal volume. For simplicity, the scatters are assumed to be spherical polystyrene beads with different diameters, and are assumed to be at a distance of 100 nm from the geometric focal point. The nonlinear coefficient and the diffraction index of the poly-bead are assumed to be 0.6 (1 + 0.5i) and 1.56, respectively. Fig. 3(b)-(d) show the induced nonlinear polarization at the focal plane (x; y; z) when spherical scatters with radii of 200 nm, 320 nm, and 400 nm are separately included in the focal volume. It is evident that the intensity of the induced polarization increases with size of the particle. The phase distributions of the nonlinear polarizations are shown in Fig. 3(f)-(h). The phase distribution is not symmetric anymore due to the effects of scattering, diffraction et al. The corresponding transfer functions are obtained and are shown in Fig. 3(j)-(m). It is found that a significant amount of energy in the distribution is still distributed in the ring, though the ring is not a symmetric one for larger diameter of the particle, and its intensity increases with the size of the diameter. Since the pinhole on the detector plane is centered on the optics axis, only a part of the energy is detected. The transverse profiles of the amplitude along the dotted lines in Fig. 3(i)-3(m) are shown in Fig. 4, which clearly indicates an increase in the detected CARS intensity with the particle size.

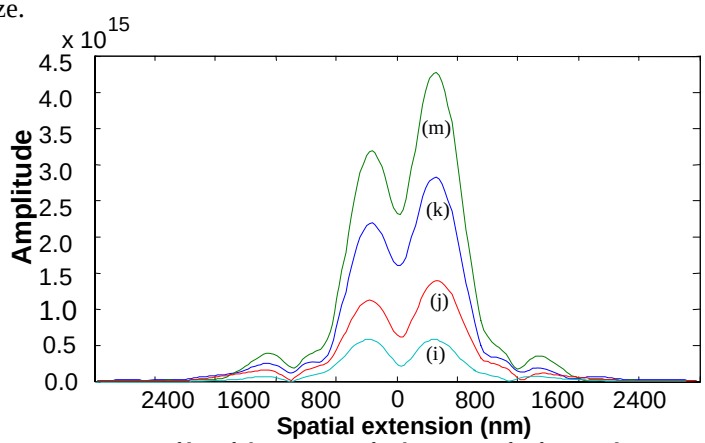

Fig. 4 Transverse profiles of the intensity of coherent transfer function lines in Fig. 3 (i)-(m) shows an increase in intensity of detection with an increase in particle size

5. Differential imaging and sensitivity

Through the analysis presented in the previous section, it is found that the bulk scattering from uniform samples such as water can be efficiently suppressed as its coherent transfer function has a distribution in the form of a ring with minimum intensity around the detection pinhole. It is also indicated that when particles are included in the focal volume, the intensity of the coherent transfer function shows an increase in detected signal with the particle size. This opens up a possibility to highlight the details of the specimen and suppress the bulk scattering. To verify this expectation, the image of a polystyrene slice in water is simulated. The polystyrene slice is assumed to be 7 um in length and width, and 0.3 um in thickness. Fig. 5(a) shows the image from a common CARS microscopy, and line-scan CARS intensity profiles along horizontal and vertical dotted lines in Fig. 7(a) are displayed in Fig. 5(c) with red lines, where the dotted and the solid lines represent intensity profiles along the horizontal and the vertical directions respectively. We can find that the contrast is a little less than 2 in Fig. 5(a); the image intensity of the polystyrene slice is 9×10^{16}, and the intensity of the water is about 6.5×10^{16}. Fig. 5(b) is the image obtained from the setup in Fig. 1. The edges of the polystyrene slice are remarkably highlighted while uniform CARS intensity inside the square of the polystyrene sample is quite much depressed. Line-scan CARS intensity profiles along horizontal and vertical dotted lines are also displayed in Fig. 5(c) with blue lines

#86014 - $15.00 USD Received 1 Aug 2007; revised 30 Aug 2007; accepted 2 Sep 2007; published 6 Sep 2007

corresponding to Fig. 5(b), where the peak intensity of the polystyrene slice edge is about 3.8×10^{15}, and the background intensity is about 1.8×10^{14}, i.e. the contrast of the image is about 20 in this case.

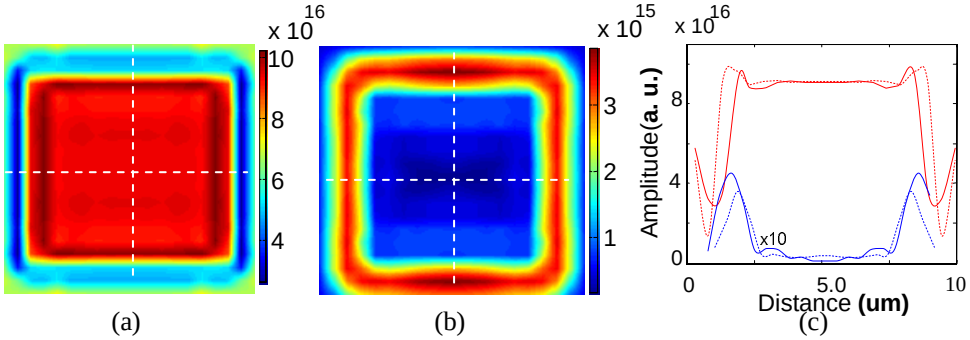

Fig. 5. Images obtained (a) without a phase modulation on the CARS signal provides a very poor edge contrast compared to (b) the image obtained with a phase modulation. The size of each image is 10 μm x10 μm. (c) Corresponding line-scan intensity profiles along the crossed lines in CARS images in (a) and (b). The blue line represents the profile of 5(b).

The proposed method indicates the possibility to highlight the sharp edges of the specimen by collecting the CARS signal with aperture modulated lens; however, practical samples include not only sharp edges but also structures of different scales. To understand the sensitivity of this method to structures of different sizes, the CARS signals are simulated with tiny scattering particles of various sizes located at the focal spot. The particles are assumed to be tiny polystyrene disks with thickness of 400 nm and radius varying from 100 nm to 1500 nm. The simulated results are shown in Fig. 6(a). It is evident from the graph (blue line) that when the size of the particle increases from zero, the signal intensity also increases and reaches its maximum when the radius is about 400 nm. A sudden decline is observed with further increase in the radius. This can be explained as follows: when the particle is small enough, the focal field keeps the symmetric phase distribution almost unchanged due to its very weak influence and a low intensity is obtained with a symmetric ring pattern centered at the axis. On the contrary, when the size is so large, it can cover the total focal spot, and the particle is essentially regarded as a bulk material, then the detected signal becomes weak. Comparing this result with that obtained in the previously reported spiral phase excitation method [11, 12], we can find that the peak intensity (green curve) occurs when the radius is about 600 nm, while that of the blue curve occurs when the radius is about 400 nm. For practical experiment, this means that the currently proposed method is suitable for visualizing smaller particles. At the same time, we can also find that the FWHM (full width at half maximum) of the blue curve is much narrower than that of the green curve. This means a more powerful size-selectivity for phase modulated collection scheme when compared to the spiral phase excitation method. Both these two phenomenon can be attributed to size difference in the focused field shown in Fig. 2. As described above and in Ref [12], while only particles with scale comparable to the focus can contribute obviously to the detected signal, the presence of any scattering particles within the focal volume can distort this ring pattern and can give rise to an increase in the detected signal as long as these particles are smaller than the size of the focus. Accordingly, when the focus of the common Gaussian beam it is used as excitation to realize differential CARS imaging, the setup in Fig. 1 is sensitive to smaller particles and has narrower response range when compared to the using of Laguerre-Gaussian beam, which has a relatively larger focus spot (see Fig. 2).

The sensitivity of the phase modulated detection is quantitatively compared with the common F-CARS microscopy (red line) and epi-detection method in Fig. 6(a). The intensity obtained in F-CARS detection is twenty times stronger than that obtained through phase

#86014 - $15.00 USD Received 1 Aug 2007; revised 30 Aug 2007; accepted 2 Sep 2007; published 6 Sep 2007

modulated collecting lens; however the intensity does not change remarkably with the size. This means a very low image contrast in a practical perspective.

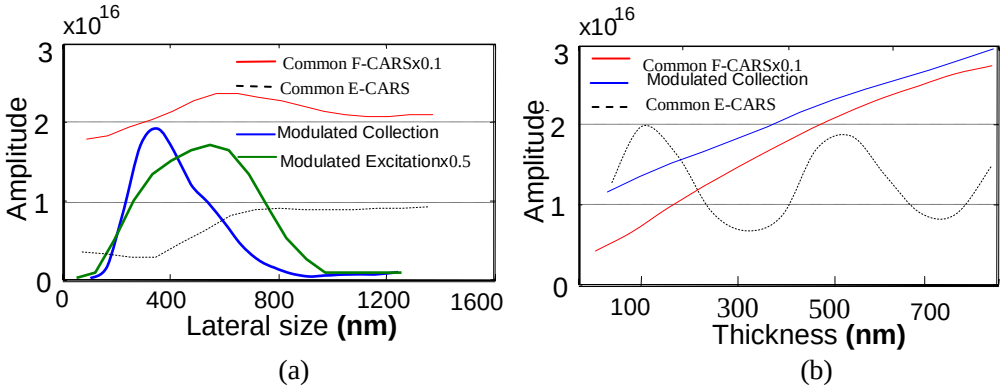

Fig. 6(a) Sensitivity of the CARS signal to the variation of particle size in the lateral direction. (b) Sensitivity of the CARS signal to the variation of particle size in the axial direction.

It has been proved both theoretically and experimentally that epi-CARS also has strong size-selectivity. However, it is sensitive only to the structures smaller than the related light wavelengths and its intensity oscillates with the diameter of the small particle [8]. As described at the beginning of this paper, this size-selectivity comes from the destructive interference between the waves emitted from different depths within the sample; in other words, it is sensitive to the particle size only along the optical axis. The common epi-CARS signal obtained with different particle size is shown in Fig. 6(a) with the broken line. As the thickness of the polystyrene slabs is fixed, and only the diameter changes in the lateral direction, the intensity of the simulated epi-CARS signal monotonously increase with the transverse diameter and shows no obvious size-selectively. In the case of phase modulated detection, the size-selectivity originates from the anti-symmetric phase distribution introduced in the focal plane with a spatial phase modulator. Thus it is only sensitive to the particle size in the lateral directions. This is the fundamental difference between the epi-detection and the focus engineering methods.

Fig. 6(b) shows the CARS signals obtained with polystyrene slabs with various thickness along the axial direction. The transverse diameter of the polystyrene slab is fixed to 400nm, and only the thickness changes in the direction of the optical axis. The simulated CARS signal obtained with the modulated collection scheme (blue line) monotonously increase with the thickness, while the intensity of the common epi-CARS signal (broken line), shows oscillations with increasing thickness. These results clearly show the difference in the size-selectivity between the schemes of the commonly used epi-detection and the focus engineering method suggested here. The red line in Fig. 6(b) is the simulated F-CARS intensity changing with the sample thickness, which also monotonously increase with the thickness and is ten times stronger than the signal obtained with spirally modulated collection scheme. Based on these results, it can be reasonably concluded that the CARS microscopy with phase modulated collection set up is much suitable and efficient for highlighting the structures with transverse scale comparable to the size of the focal spot. When the size of the structure is much larger or smaller than the focal spot in the lateral directions, the sensitivity of this method decreases.

6. Discussions and Conclusion

CARS generation and phase modulated detection are numerically studied using a rigorous simulation based on FDTD method. The background signal from a homogenous bulk sample is completely suppressed by modulating the CARS signal into a ring pattern and using a confocal detection system. The presence of any scattering particles within the focal volume

#86014 - $15.00 USD Received 1 Aug 2007; revised 30 Aug 2007; accepted 2 Sep 2007; published 6 Sep 2007

can distort this ring pattern and can give rise to an increase in the detected signal through the pinhole, thus the fine structure of the sample can be efficiently highlighted. The illumination can be still Gaussian without any loss in intensity and spatial resolution at the focal point as the signal is modulated only at the collecting lens. It is also found that this method is much suitable for highlighting the specimen details with scale comparable to the focal spot of the system while suppressing the non-resonant background signal. The numerical investigation is done considering the effects of scattering, near-field waves, index-mismatch, and diffraction.

Spiral phase modulator has been used earlier to realize differential images in common microscopy, where the non-uniformity of the refractive index and transmittance of the sample are the main reasons for highlighting the fine structures [18, 19]. However, most of the samples being examined in CARS microscopy are very thin bio-slice or cultured cell. These kinds of bio-samples are almost uniformly transparent, and their index is always around 1.35. Thus it is reasonable for them to be considered as uniform in terms of index and transmittance within the focal volume, which can be only about tens nanometers in both the lateral and axial directions. Based on this approximation, the detected differential image is mainly due to the discontinuity of the nonlinearity $\chi^{(3)}$ in the lateral directions, and accordingly the interpretation of the CARS image in practical experiments becomes easy. Since the strong CARS signal can be obtained only at positions where the nonlinearity of the sample varies rapidly in the transverse directions, the brightest area in the detected differential image always indicates an interface between different organelles, such as plasma membrane, cell wall et al, and the cytosol and the nucleoplasm will appear to be dark areas on the detected image due to its uniformity in component. Taking a lipid droplet as an example, it appears to be a bright round disk on common CARS images; however, it will become a closed bright circle in the differential image.

Acknowledgments

This work was supported by the Creative Research Initiatives (CRI) Program of Korea Science and Engineering Foundation (KOSEF) / Ministry of Science and Technology (MOST).

#86014 - $15.00 USD Received 1 Aug 2007; revised 30 Aug 2007; accepted 2 Sep 2007; published 6 Sep 2007